

# Bond disorder enhances the information transfer in polar flock

Jay Prakash Singh<sup>1,\*</sup> Sameer Kumar<sup>2,†</sup> and Shradha Mishra<sup>1‡</sup>

<sup>1,2</sup>*Department of Physics, Indian Institute of Technology (BHU), Varanasi, India 221005*

(Dated: March 19, 2022)

Collection of self-propelled particles (SPPs) exhibit coherent motion and show *true* long-range order in two-dimensions. Inhomogeneity, in general destroys the usual long-range order of the polar SPPs. We model a system of polar self-propelled particles with inhomogeneous interaction strength or *bond disorder*. The system is studied near the order-to-disorder transition for different strengths of the disorder. The nature of phase transition changes from discontinuous to continuous type by tuning the strength of the disorder. The bond disorder also enhances the ordering near the transition due to the formation of a homogeneous flock state for the large disorder. It leads to faster information transfer in the system and enhances the system's information entropy. Our study gives a new understanding of the effect of intrinsic inhomogeneity in the self-propelled particle system.

## I. INTRODUCTION

Collective behavior of a large number of self-propelled particles (SPPs) or “flocking” is ubiquitous. Examples of such systems range from a few micrometers, e.g., actin and tubulin filaments, molecular motors [1, 2], unicellular organisms such as amoebae and bacteria [3], to several meters, e.g., bird flock [4], fish school [5] and human crowd [6] *etc.* Interestingly, these systems show a collective motion on a scale much larger than each individual, and hence long-range ordering (LRO) is observed in two-dimensional.

A minimal model for understanding the basic features of the collective behavior of polar self-propelled particles or “polar flock” was introduced in 1995 by T. Vicsek *et al.* [7]. In the last three decades, many variants of the Vicsek model are studied to understand various features of different model systems [9–12].

In these studies, authors mainly consider a collection of SPPs in a homogeneous system or medium. Recently, there is a growing interest to understand the effects and advantages of different kinds of inhomogeneities, which are omnipresent in nature. Many studies show that the inhomogeneity can destroy the LRO present in a clean system [13–21] whereas a few studies discuss special kinds of inhomogeneities that enhance the ordering in the system [22, 23]. Therefore, the inhomogeneity can be useful for many practical applications, e.g., crowd control and faster evacuation *etc.*[24, 27–32].

In the Vicsek model, each individual interacts through a short-range alignment interaction and the strength of the interaction is the same for all the particles. But in natural systems, each particle can have a different ability to influence its neighbors based on their individual intelligence or physical strength, *etc.* However, scientists have not paid much attention to understand the effects of different interaction strengths in a polar flock. In a recent study, William *et al.* show that the varying

interaction strength of the SPPs results in maximum entropy. Hence, more information transfer among the particles [33][43]. Surprisingly, in this work, we note that the presence of inhomogeneity in the form of the particles' different interaction ability, the system approaches a more homogeneous state near to the point of order-disorder transition. More importantly, the flock's response is faster for higher disorder in the interaction strength among the SPPs because each SPP neighbor is updated more frequently, which leads to faster information transfer within the flock. We also calculate the information entropy [44–46] for different disorder and find that the larger the disorder more is the information entropy of the system.

We also characterised the effect of bond disorder on the nature disorder-to-order phase transition in the system. Which is a matter of great interest in many previous studies [10, 11]. We find that the nature of disorder-to-order phase transition changes from discontinuous type to continuous type by tuning the strength of bond disorder. Also, the system shows the enhanced ordering near the transition point for the larger disorder.

The rest of the paper is organized as follows. In Sec.II, we discuss the model and simulation details. In Sec.III, the results from the numerical simulations are discussed. In Sec.IV, we conclude the paper with a summary and discussion of the results.

## II. MODEL

We consider a collection of  $N$  polar self-propelled particles (SPPs) moving on a two-dimensional substrate. SPPs interact through a short-range alignment interaction within a small interaction radius  $R_I$  [7, 9, 10]. Moreover, the strength of interaction of each SPP with its neighbors is *different*, unlike the Vicsek model [7] of uniform interaction strength. Each SPP is defined by its position  $\mathbf{r}_i(t)$  and orientation  $\theta_i(t)$ , and it moves along its direction vector  $\mathbf{n}_i(t) = (\cos(\theta_i(t)), \sin(\theta_i(t)))$  with a fixed speed  $v_0$ . The two update equations for the position  $\mathbf{r}_i(t)$  and the direction vector  $\mathbf{n}_i(t)$  are given by,

$$\mathbf{r}_i(t + \Delta t) = \mathbf{r}_i(t) + v_0 \mathbf{n}_i(t) \Delta t \quad (1)$$

\* jayps.rs.phy16@itbhu.ac.in

† samkum2010@gmail.com

‡ smishra.phy@itbhu.ac.in

$$\mathbf{n}_i(t + \Delta t) = \frac{\sum_{j \in R_I} J_j \mathbf{n}_j(t) + \eta N_i(t) \xi_i(t)}{w_i(t)} \quad (2)$$

The first equation represents the particle's motion due to its self-propelled nature, along the direction vector  $\mathbf{n}_i(t)$  with fixed speed  $v_0$ .  $\Delta t = 1.0$  is the unit time step. The first term in Eq.2 represents the short-range alignment interaction of the  $i^{\text{th}}$  particle with its neighbors within the interaction radius ( $R_I$ ), and  $J_j$  is the interaction strength of the  $j^{\text{th}}$  neighbor. The probability distribution of the interaction strength  $J$ ,  $P(J)$ , is obtained from a uniform distribution of range  $[1 - \frac{\epsilon}{2} : 1 + \frac{\epsilon}{2}]$  [35], where  $\epsilon$  measures the degree of disorder.  $\epsilon = 0$  corresponds to the uniform interaction strength ( $J_i = 1$  for all the particles) like the Vicsek model [7] whereas  $\epsilon = 2$  corresponds to the maximum disorder in the system.

Furthermore, the second term in the Eq.2 denotes the vector noise, which measures the particle's error while following its neighbors.  $\xi_i(t)$  is a random unit vector, where  $N_i(t)$  denotes the number of neighbors within the interaction radius of the  $i^{\text{th}}$  particle at time  $t$ .  $\eta$  represents the strength of the noise and can vary from 0 to 1.  $w_i(t)$  is the normalization factor, which reduces the right-hand side of the Eq.2 to a unit vector.

For zero self-propulsion speed model reduces to the *equilibrium* random bond XY-model [25, 26]. However, for  $\epsilon = 0$ , the model reduces to the *clean* polar flock. We numerically update the Eqs.1 and 2 for all SPPs sequentially. One simulation step is counted after the update of Eqs.1 and 2 once for all the particles. Periodic boundary condition (PBC) is used for a system of size  $L \times L$ , and  $L$  is taken as 100, 150. The number density of the system is defined as  $\rho_N = \frac{N}{L \times L}$ . We fix the density at  $\rho_N = 1.0$  and self-propulsion speed  $v_0 = 0.5$ . Since for the same density for the clean polar flock, the critical noise is close to  $\eta \sim 0.6$ , we limit our study near to the critical point, and the noise strength is varied from  $\eta = 0.4 - 0.8$  to study the phase transition and  $\eta$  is fixed 0.62 to characterised the properties of polar flock near to critical point. The study deep in the ordered state  $\eta < 0.4$  is also interesting and recently studied in [50]. We considered time up to  $10^6$  and 20 independent realizations to study the steady-state results.

### III. RESULTS

#### A. Disorder-to-order transition

First, we study the disorder-to-order transition in the system for different disorder strengths  $\epsilon$ . Ordering in the system is characterized by the mean orientation order parameter,

$$\chi(t) = \frac{1}{N} \left| \sum_i^N n_i(t) \right| \quad (3)$$

In the ordered state, i.e., when majority of particles are moving in the same direction, then  $\chi$  will be closer to 1,

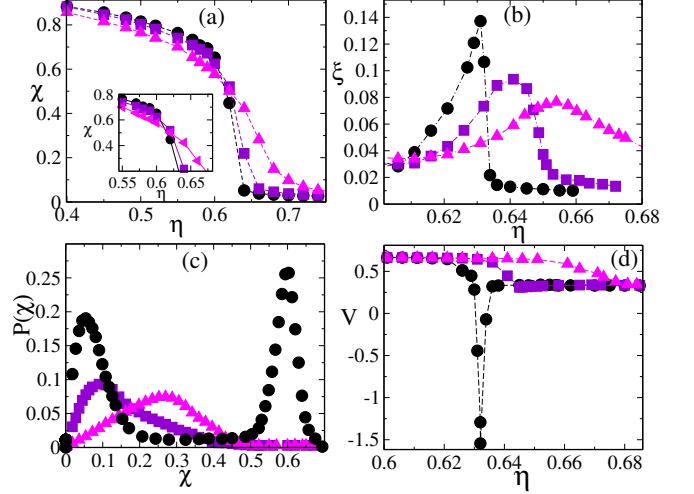


FIG. 1. (color online) (a) Plot of the mean orientation order parameter  $\chi$  vs. noise strength  $\eta$ , *inset*: zoomed plot shows enhance ordering on increasing  $\epsilon$ . (b) Variation of susceptibility  $\xi$  vs.  $\epsilon$ . (c) The probability distribution function of order parameter  $P(\chi)$  vs.  $\chi$  at the transition point ( $\eta_c(\epsilon) = 0.625, 0.640, 0.654$  for  $\epsilon = 0, 1$  and  $2$  respectively). (d) Variation of fourth-order binder cumulant  $V$  vs.  $\eta$ . Different symbols implies different values of disorder strength  $\epsilon = 0$  (circles),  $1.0$  (squares),  $2.0$  (triangles) for the system size  $N=22,500$  and the density  $\rho = 1.0$ .

and of the order of  $\frac{1}{\sqrt{N}}$  for a random disordered state. In Fig.1(a) we have shown the variation of  $\chi(t)$  with the noise strength  $\eta$  for three different  $\epsilon = (0, 1, 2)$ . For  $\epsilon = 0$ , the variation of  $\chi$  shows a sharp change from  $\chi \sim 1$  to  $\sim 0$ . This kind of change is a common feature of first-order phase transition [10–14]. Whereas for  $\epsilon = 2$ ,  $\chi$  varies continuously, and the transition has a signature of second-order phase transition. The variation of  $\chi$  for  $\epsilon = 1$ , it shows the intermediate behaviour. The plot of order parameter fluctuation or the susceptibility  $\xi = \sqrt{\langle \chi^2 \rangle - \langle \chi \rangle^2}$ , is shown in Fig. 1(b), where  $\langle . \rangle$  denotes the average over steady-state time. The critical noise  $\eta_c$  is obtained from the maximum of  $\xi$ . The  $\eta_c(\epsilon)$  shifts towards right on increasing  $\epsilon = 0, 1$  and  $2$  respectively. To further understand the nature of phase transition, we plot order parameter probability distribution function (PDF)  $P(\chi)$  vs.  $\chi$  in Fig.1(c) at the critical noise  $\eta_c(\epsilon) = 0.625, 0.640, 0.654$  for three  $\epsilon = 0, 1$  and  $2$  respectively. For  $\epsilon = 0$ , there is a clear bimodal nature of  $P(\chi)$  gradually changes to unimodal on increasing  $\epsilon$ . To further characterise the nature of the transition for  $\epsilon = (0, 1, 2)$  in Fig.1 (d), we calculate the fourth-order cumulant or the Binder cumulant  $V = 1 - \frac{\langle \chi^4 \rangle}{3 \langle \chi^2 \rangle^2}$  vs.  $\eta$ . We plot  $V(\eta)$  versus  $\eta$  in Fig.1(d). It shows strong discontinuity between  $V = 1/3$  (for disordered state) to  $V = 2/3$  (for ordered state) as we approach critical  $\eta_c$  for  $\epsilon = 0$ ; however, it smoothly goes between a disordered state ( $V = 1/3$ ) to an ordered state ( $V = 2/3$ ) for  $\epsilon = 2$ . Now we try to understand the shift in critical noise strength  $\eta_c$  towards higher values, as well as enhanced ordering near  $\eta = 0.6$

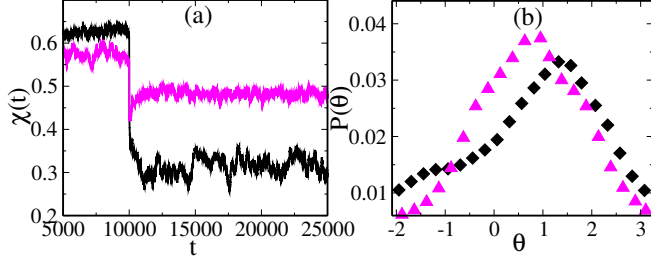


FIG. 2. (color online) (a) Time series of  $\chi(t)$  for disorder  $\epsilon = 1.0$  (black line) and  $\epsilon = 2.0$  (magenta line). The two types of quenched impurities with orientations  $\pm\frac{\pi}{2}$  are introduced at time  $t = 10,000$ . (b) PDF for the orientation distribution  $P(\theta)$  vs. mean orientation  $\theta$ , for  $\epsilon = 1.0$  (squares) and  $\epsilon = 2.0$  (triangles). All the plots are for system size  $N = 10,000$ , noise strength  $\eta = 0.62$  and the density  $\rho = 1.0$ .

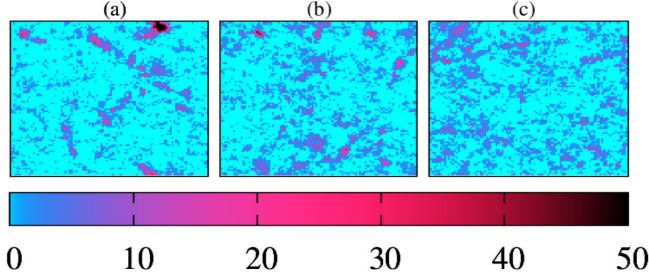


FIG. 3. (color online) Plot (a), (b) and (c) are the realspace snapshots for three  $\epsilon = 0, 1$  and  $2$  respectively. colorbar shows intensity with respect to particle clusters. All the parameters are same as in Fig. 2.

for the higher disorder, as shown in the zoomed-in plot in Fig. 1(a).

To understand the enhanced ordering mechanism, we perform a small perturbative study on the system. Since we find enhanced ordering near  $\eta \sim 0.6$ , the perturbation is imposed at  $\eta = 0.62$  for finite disorder  $\epsilon = 1$  and  $2$ .

In the perturbative study, the system is waited to reach to the steady-state ( $t = 10^4$ ) and once the steady-state is reached; as shown in Fig. 2(a), we choose 5% of the particles randomly and out of which the direction of 2.5% particles with  $J > 1$  quenched to the direction  $\frac{\pi}{2}$  and another 2.5% with  $J < 1$  are quenched to the direction  $-\frac{\pi}{2}$ . Once this perturbation is applied, the system will respond to it and mean order parameter  $\chi(t)$  shows a dip and then relaxes to a new steady state with relatively lower value of  $\chi(t)$  as shown in Fig. 2(a). Very clearly before perturbation,  $\chi$  is lower for  $\epsilon = 2$ , hence a more ordered state for the lower disorder. But after perturbation, which is selectively for particles with higher and lower  $J$  values, the response is different for  $\epsilon = 1$  and  $2$ . For  $\epsilon = 2$ , after perturbation  $\chi$  is larger compare to  $\epsilon = 1$ . Hence more ordered state for the larger disorder. In the plot of Fig.2(b) we plot the orientation probability distribution function (PDF)  $P(\theta)$  of the particles orientation  $\theta$ . For  $\epsilon = 1$ , the  $P(\theta)$  shows two distinct peaks for  $\theta = \pm\pi/2$ , but peak for

$\pi/2$  or response to higher  $J$  is more. For  $\epsilon = 2$ , the mean of the total  $P(\theta)$  shifts towards the non-zero  $\theta$ , hence the system's response happens globally, and the whole system is polarised in the direction of quenched particles with larger  $J$  values.

Now we further study the consequence of such enhanced ordering for larger disorder on the polar flock. Moreover, this dominated alignment is responsible for shifting of transition point  $\eta_c$  towards higher values.

## B. Properties of polar flock

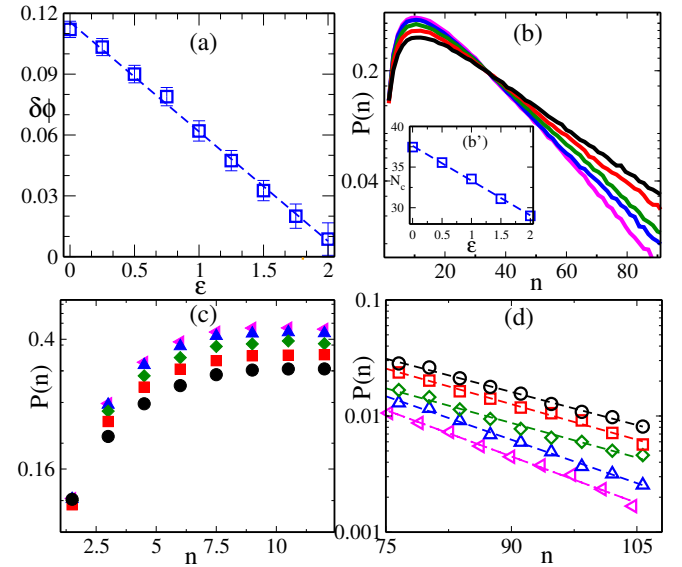


FIG. 4. (color online) (a) Plot of density phase separation order parameter  $\delta\phi$  vs.  $\epsilon$  with blue squares. Blue dotted line shows linear decay of  $\delta\phi$  (b)  $P(n)$  vs.  $n$  for  $\epsilon = 0, 0.5, 1, 1.5$  and  $2$  respectively. Different colors with line black, red, green, blue and magenta are for  $\epsilon = 0, 0.5, 1, 1.5$  and  $2$ . Inset of Fig.(b) shows the mean number of particles  $N_c$  vs.  $\epsilon$  where blue dotted line shows linear decay of  $N_c$ . (c) and (d) show the zoom plot of (b) near to the head and tail where tail part are fitted with exponential function with dotted lines. Symbols with black(circles), red(squares), green(diamonds), blue(triangles up) and magenta(triangles left) colors are for  $\epsilon = 0, 0.5, 1, 1.5$  and  $2$  in (c) and (d). Also (b), (c) and (d) are in semi-log y-axis. All the parameters are same as in Fig. 2.

How disorder affects the density fluctuations in the system? We plot realspace snapshot of the local density (calculated in small region of unit size square sub-shell), in Fig.3(a)-(c) for three values of  $\epsilon = (0, 1$  and  $2)$  at time  $t = 10^5$ . For clean polar flock,  $\epsilon = 0$ , particles form isolated clusters. Whereas with a non-zero  $\epsilon$ , these isolated clusters break, and the system gets into a more homogeneous state. To further confirm this, we calculate the density phase separation order parameter,  $\delta\phi$  vs.  $\epsilon$  (where  $\delta\phi(\epsilon)$  is the deviation of the number of particles among the sub-cells), Fig.4(a). We calculate

$\delta\phi$  by dividing the whole  $L \times L$  system into unit sized sub-cells,  $\delta\phi(\epsilon) = \sqrt{\frac{1}{L^2} \sum_{j=1}^{L^2} (\phi_j(\epsilon))^2 - (\frac{1}{L^2} \sum_{j=1}^{L^2} \phi_j(\epsilon))^2}$  where  $\phi_j$  is the number of particles in the  $j^{\text{th}}$  sub-cell and  $\langle \dots \rangle$  represents averaging over 20 realisations. We note that  $\delta\phi$  decreases in a linear fashion with increasing  $\epsilon$  as shown in Fig. 4(a). Hence system becomes more homogeneous with increasing the random bond disorder  $\epsilon$  in the system. Furthermore, in Fig.4(b) we plot the probability distribution function (PDF) of number of neighbours  $P(n)$  for different values of  $\epsilon = 0, 0.5, 1, 1.5$  and 2 respectively. Sharper tail for large  $n$  for higher value of  $\epsilon = 2$  shows that the system is approaching towards more homogeneous state or clusters of smaller size while longer tail, for lower values of  $\epsilon = 0$  hence bigger clusters. In the inset of Fig.4(b) we plot the mean number of particles  $N_c$  with  $\epsilon$  where  $N_c$  is obtained by fitting the tail of the main plot by the exponential function  $\exp(-\frac{n}{N_c})$ . This shows that  $N_c$  decreases linearly with an increase in the value of  $\epsilon$ . Similarly when zoomed for smaller  $n$  as shown in Fig. 4(c),  $P(n)$  for larger  $\epsilon$  is higher as compare to smaller  $\epsilon$ . Hence small clusters have more probability for larger disorder. Fig. 4 (d) the zoomed tail of the  $P(n)$ .

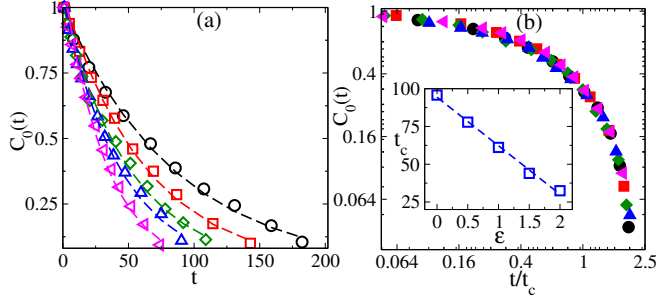


FIG. 5. (color online) (a) Plot of OACF  $C_0(r, t)$  vs.  $t$ . for  $\epsilon = 0.0$  (circles),  $0.5$  (squares),  $1.0$  (diamonds),  $1.5$  (triangles up) and  $2.0$  (triangles left). Dashed lines are fit to exponential to the data (symbols). (b) Plot for  $C_0(r, t)$  vs. scaled time  $t/t_c$ ; and  $t_c$  vs.  $\epsilon$  (inset) where the dashed lines is linear fit to the data. All other parameters are same as in Fig. 2

### C. Accelerated response to external perturbation

We claim that enhanced ordering near-critical region and homogeneous density clusters promote faster information transfer among the flock. To confirm the same we perform another perturbation to the well-ordered flock in the steady state and calculate its response. We randomly select a fraction of particles 1% and quench their direction to a randomly selected fixed orientation. With time all other particles will rotate in that direction. Their response to the direction of quench is measured by calculating the orientation auto-correlation function (OACF)  $C_0(t) = \langle \cos \theta_i(t) - \theta_i(0) \rangle - \langle \cos \theta_i(T) - \theta_i(0) \rangle$ .

Where  $\theta_i(t)$  and  $\theta_i(0)$  are the orientation of the  $i^{\text{th}}$  particle at time  $t$  and 0 from the time of quench and  $T$  is

the late time when approximately all the particles are oriented in the direction of the quench.  $\langle \dots \rangle$  denotes averaging over all the SPPs and 30 independent realizations.

In the Fig.5 (a) OACF  $C_0(t)$  decay exponentially and show the sharper decay with increase in the strength of disorder  $\epsilon$ . Therefore, the response of the flock to external perturbation becomes faster, with the increase in  $\epsilon$ . In Fig. 5(b) we plot the  $C_0(t)$  vs. scaled time  $t/t_c$ , where  $t_c$  is obtained from the fitting of  $C_0(t)$  to  $\exp(-t/t_c)$ . The inset of Fig. 5(b), shows the variation of  $t_c$  vs.  $\epsilon$ .  $t_c$  shows linear decay with  $\epsilon$ , which confirms the faster response of the flock towards external perturbation with an increase in the value of  $\epsilon$ .

### D. Disorder increases system's information entropy

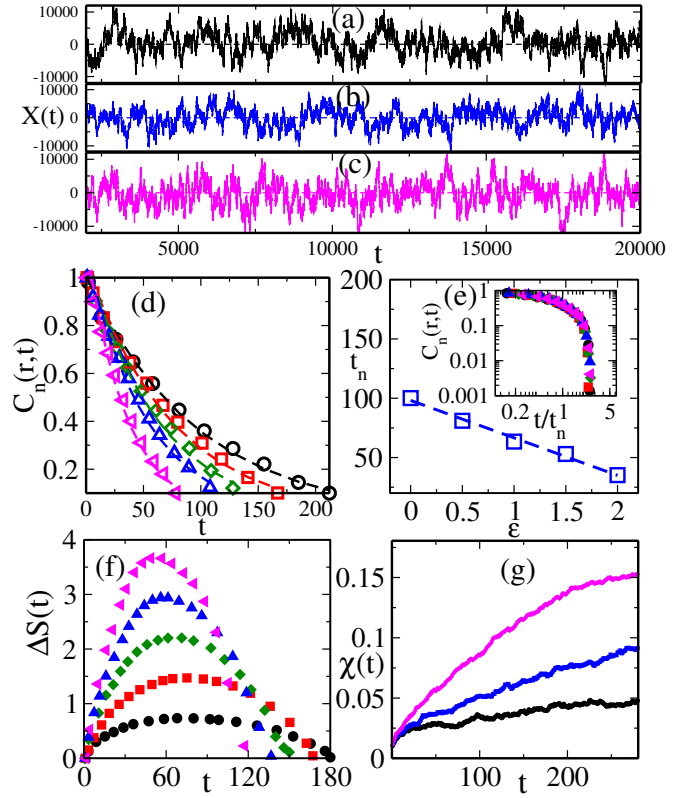


FIG. 6. (color online) (a), (b) and (c) shows the variation of  $X(t)$  vs.  $t$ . Black, blue and magenta colors are for  $\epsilon = 0, 1$  and  $2$  respectively. (d) Variation of neighbour fluctuation autocorrelation  $C_n(r, t)$  vs.  $t$ . Symbols with black (circles), red (squares), green (diamonds), blue (triangles up) and magenta (triangles left) colors are for  $\epsilon = 0, 0.5, 1, 1.5$  and  $2$  respectively. Dashed lines are fit to exponential. (e) Plot of  $t_n$  vs.  $\epsilon$  shows linear decay with  $\epsilon$ ; inset; plot of correlation  $C_n(r, t)$  vs. scaled time  $t/t_n$ . (f) Plot of information entropy  $\Delta S(t)$  vs.  $t$ . (g) Time evolution of  $\chi(t)$  with time  $t$  where colors black, blue and magenta are for  $\epsilon = 0, 1$  and  $2$  respectively. All other parameters are the same as in Fig. 2

Further, we claim that the accelerated response to external perturbation is due to neighbors' frequent updates for high disorder strength.

We define the update in the neighbour list of the SPPs as  $X(t) = \frac{1}{N} \sum_{i=1}^N ((N_R^i(t) \times N/2) - \sum_{j \in R} j)$ . where  $N_R^i$  is the number of SPPs inside the interaction radius of the  $i^{th}$  particle,  $N$  is the total number of particles in the system, and the second term on the right-hand side is the sum over all the particle indices  $j$  inside the interaction radius of the  $i^{th}$  particle. The time series of  $X(t)$  oscillates around 0 for different values of  $\epsilon$ , as shown in Fig.6(a),(b) and (c). The frequency of oscillation of  $X(t)$  increases with increasing  $\epsilon$ . The increase in the oscillation frequency of  $X(t)$  suggests more frequent updates of the neighbor list, and the decrease in the magnitude of  $X(t)$  implies a lesser number of neighbors inside the interaction radius of an SPP. Furthermore, we calculate the neighbor autocorrelation function,

$$C_n(t) = \left\langle \frac{\sum_{t'=1}^{T-t} (X(t') - \bar{X})(X(t'+t) - \bar{X})}{\sum_{t'=1}^T (X(t') - \bar{X})^2} \right\rangle \quad (4)$$

where  $\bar{X}$  is the mean value of  $X(t)$  over the total time  $T$  and  $t < T$ .  $\langle \dots \rangle$  represents averaging over 20 independent realisations. In Fig.6(d) faster decay of  $C_n(t)$  with increase the disorder strength  $\epsilon$ , suggest more frequent update of neighbour list. Also in the inset of Fig.6(e) we plot the scaled correlation  $C_n(t)$  vs.  $t/t_n$  where  $t_n$  is obtained by fitting the exponential function to  $\exp(-\frac{t}{t_n})$ . In the Fig.6(e) we have shown the variation of  $t_n$  with  $\epsilon$ , which decays linearly. Now use the information entropy [44, 47] approach to show that the larger the disorder, the larger is the information entropy and hence the more information transfer among the SPPs. The faster information transfer in more disorder system is due to the possibility of more number of accessible states for the particles. Each state can be defined as the new neighbors in the chosen particle's contact list. If we denote  $P_s$ , as the probability of being in the  $i^{th}$  states from the set of all possible accessible states.

If a particle changes its neighbors frequently, then it is exploring more number of neighboring particles and hence more number of states. Hence the neighbor autocorrelation,  $C_{n,s}(t)$ , ( the quantity inside the  $\langle \dots \rangle$  of Eq. 4) is the neighbour autocorrelation for one state. The subscript  $s$  denotes the different independent configurations and hence different sets can be generalised as different independent configurations. And  $C_{n,s}(t)$  and  $P_s(t)$  are equivalent. One is the measure of probability of being in a given neighbour list and is the same as  $P_s(t)$ . As time progress  $C_{n,s}(t)$  decreases hence more and more states are accessed. Hence we define the information entropy of the system as  $\Delta S(t) = -\sum_s C_{n,s}(t) \ln_2 C_{n,s}(t)$ , where summation  $s$  is over all possible realisations. Larger the information entropy larger the available microstate for the particles and hence the more information transfer among the flocks. We plot the variation of information entropy  $\Delta S(t)$  for different disorder in Fig. 6(f). We note that  $\Delta S(t)$  increases with  $\epsilon$ , which further

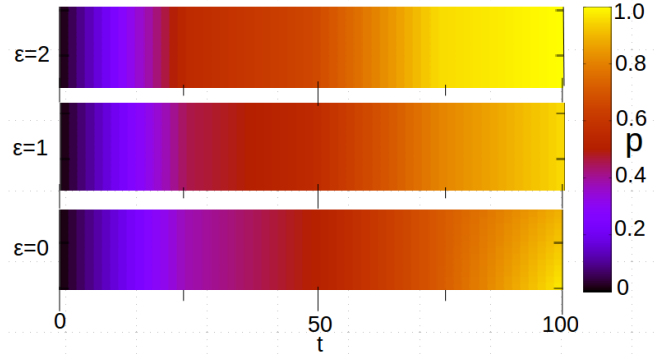


FIG. 7. (color online) Top to bottom color plot shows the probability of newly visited particles  $p$  for three  $\epsilon = 2, 1$  and  $0$  with time. All other parameters are same as in Fig. 2

confirms that particles are exploring the more states for higher disorder strength hence more information transfer. Also, in fig.6(g), we have plotted the time evolution of order parameter in the early time, which shows that for larger  $\epsilon$ , the system reaches the ordered state quicker in comparison to the lower  $\epsilon$ .

Further, we also show the quicker update of neighbour list for a single particle. In Fig. 7, we plot the fraction of new particles  $p(\epsilon, t)$  in the neighbour list of a given particle from some reference time  $t_0 = 0$ . At time  $t_0$ , all the particles are labeled as old hence  $p = 0$ . As time progress new particles come in the contact list of the given particle and  $p$  starts to increase. At very late time all the old particles are gone out of the neighbour list and hence  $p = 1$ . As shown in the figure, for larger disorder new neighbours are updated faster than for the small disorder.

#### IV. DISCUSSION

We introduced a minimal model for a collection of self-propelled particles with bond-disorder. Each particle has a different ability (interaction strength) to influence its neighbors. The varying interaction strength is obtained from a uniform distribution, and it can be varied from  $[1 - \epsilon/2 : 1 + \epsilon/2]$ , where  $\epsilon$  is the disorder strength. For  $\epsilon = 0$ , the model reduces to the constant interaction strength model or the Vicsek-like model [7]. We studied the steady-state characteristics for different strengths of the disorder near to order-disorder transition. To our surprise, bond disorder leads to faster information transfer within the flock, viz; the system's information entropy gets increased.

We also find that the disorder-to-order transition is discontinuous in the disorder free system and changes to continuous type with an increase in disorder. Furthermore, the transition point shifts towards the higher  $\eta$  for the large disorder.

Our study provides a new direction to understand the effect of intrinsic inhomogeneity in many natural active

systems. It shows that how the bond-disorder in the system can enhance ordering and faster information transfer among the particles. Such properties can be useful for many applications: like the faster evacuation of active particles and also for crowd control in many social gatherings [48, 49]

## V. ACKNOWLEDGEMENT

SM and SK, thanks DST-SERB India, ECR/2017/000659 for the financial support. The

support and the resources provided by PARAM Shiva<sup>6</sup> Facility under the National Supercomputing Mission, Government of India at the Indian Institute of Technology, Varanasi are gratefully acknowledged. Computing facility at Indian Institute of Technology(BHU), Varanasi is gratefully acknowledged.

- 
- [1] F. Nédélec, Ph.D. thesis, Université Paris **11**, 1998; F. Nédélec, T. Surrey, A. C. Maggs, and S. Leibler, *Nature (London)* **389**, 305 (1997).
- [2] H. Yokota (private communication); Y. Harada, A. Noguchi, A. Kishino, and T. Yanagida, *Nature (London)* **326**, 805 (1987); Y. Toyoshima et al., *Nature (London)* **328**, 536 (1987); S. J. Kron and J. A. Spudich, *Proc. Natl. Acad. Sci. U.S.A.* **83**, 6272 (1986).
- [3] J. T. Bonner, *Proc. Natl. Acad. Sci. U.S.A.* **95**, 9355 (1998); M. T. Laub and W. F. Loomis, *Mol. Biol. Cell* **9**, 3521 (1998).
- [4] D. Chen, Y. Wang, G. Wu, M. Kang, Y. Sun, and W. Yu, *Chaos* **29**, 113118 (2019).
- [5] *Three Dimensional Animals Groups*, edited by J. K. Parrish and W. M. Hamner (Cambridge University Press, Cambridge, England, 1997).
- [6] D. Helbing, I. Farkas, and T. Vicsek, *Nature (London)* **407**, 487 (2000).
- [7] T. Vicsek, A. Czirók, E. Ben-Jacob, I. Cohen, and O. Shochet, *Phys. Rev. Lett.* **75**, 1226 (1995).
- [8] J. Toner and Y. Tu, *Phys. Rev. E* **58**, 4828 (1998).
- [9] G. Grégoire and H. Chaté, *Phys. Rev. Lett.* **92**, 025702 (2004).
- [10] H. Chaté, F. Ginelli, Guillaume Grégoire, and F. Raynaud, *Phys. Rev. E* **77**, 046113 (2008).
- [11] S. Pattanayak and S. Mishra, *Journal of Physics Communications*, **2**, 045007 (2018).
- [12] M. Romensky, V. Lobaskin, and T. Ihle, *Phys. Rev. E* **90**, 063315 (2014).
- [13] A. Morin, N. Desreumaux, J. Caussin, and D. Bartolo, *Nature Physics* **13**, 63–67 (2017).
- [14] O. Chepizhko, E. G. Altmann, and F. Peruani, *Phys. Rev. Lett.* **110**, 238101 (2013).
- [15] D. Yllanes, M. Leoni, and M. C. Marchetti, *New Journal of Physics* **19**, 103026 (2017).
- [16] D. A. Quint and A. Gopinathan, *Phys. Biol.* **12**, 046008 (2015).
- [17] C. Sándor, A. Libál, C. Reichhardt, and C. J. Olson Reichhardt, *Phys. Rev. E* **95**, 032606 (2017).
- [18] C. J. O. Reichhardt and C. Reichhardt, *Nat. Phys.* **13**, 10 (2017).
- [19] R. Das, M. Kumar, and S. Mishra, *Phys. R. E.* **98**, 060602(R) (2018).
- [20] J. Toner, N. Guttenberg, and Y. Tu, *Phys. Rev. E* **98**, 062604 (2018).
- [21] J. Toner, N. Guttenberg, and Y. Tu, *Phys. Rev. Lett.* **121**, 248002 (2018).
- [22] R. Das, M. Kumar, and S. Mishra, *Phys. Rev. E* **101**, 012607 (2020).
- [23] S. Pattanayak, M. Kumar, and S. Mishra, arXiv:2001.06584 (2020).
- [24] Guo-yuan Wang, Fan-yu Wu, You-liang Si, Q. Zeng, and P. Lin, *Procedia Engineering* **211**, 699 (2018).
- [25] Vik. S. Dotsenko and M. V. FeTgel man, *Zh. Eksp. Teor. Fiz.* **83**, 345 (1982).
- [26] M. Kumar, S. Chatterjee, R. Paul, and S. Puri, *Phys. Rev. E* **96**, 042127 (2017).
- [27] G. A. Frank and C. O. Dorso, *Physica A (Amsterdam, Neth.)* **390**, 2135 (2011).
- [28] A. Garcimartín, D. R. Parisi, J. M. Pastor, C. Martín-Gómez, and I. Zuriguel, *J. Stat. Mech.* **4**, 043402 (2016).
- [29] I. Zuriguel, J. Olivares, J. M. Pastor, C. Martín-Gómez, L. M. Ferrer, J. J. Ramos, and A. Garcimartín, *Phys. Rev. E* **94**, 032302 (2016).
- [30] J.P. Singh and S. Mishra *Physica A* **544** (2020) 123530
- [31] S Kumar, S Mishra arXiv:2002.10805 [cond-mat.soft]
- [32] I. Zuriguel, A. Janda, A. Garcimartín, C. Lozano, R. Arévalo, and D. Maza *Phys. Rev. Lett.* **107**, 278001 (2011).
- [33] W. Bialek, A. Cavagna, I. Giardina, T. Mora, E. Silvestri, M. Viale, and A. M. Walczak, *PNAS* **109**, 4786 (2012).
- [34] Vik. S. Dotsenko and M. V. FeTgel man, *Zh. Eksp. Teor. Fiz.* **83**, 345 (1982).
- [35] M. Kumar, S. Chatterjee, R. Paul, and S. Puri, *Phys. Rev. E* **96**, 042127 (2017).
- [36] D. J. Bishop and J. D. Reppy, *Phys. Rev. Lett.* **40**, 1727(1978).
- [37] A. J. Bray, *Advances in Physics* **43**, 357 (1994).
- [38] S. Puri, and V. Wadhawan, *Kinetics of Phase Transitions*, CRC press (2009).
- [39] R. Wittkowski, A. Tiribocchi, J. Stenhammar, R. J. Allen, D. Marenduzzo, and M. E. Cates, *Nature Communications* **5**, 4351 (2014).
- [40] S Pattanayak, S Mishra, S Puri - arXiv preprint arXiv:2101.10626, 2021.
- [41] B. Bhattacharjee, S. Mishra, S.S. Manna, *Phys. Rev. E.* **92**, 062134 (2015).
- [42] C. P. Beatrici, R. M. C. de Almeida, and L. G. Brunnet, *Phys. Rev. E.* **95**, 032402 (2017).
- [43] S. Pattanayak, JP Singh, M Kumar, S. Mishra *Phys. Rev E.* **101** 052602(2020)
- [44] Andrea Cavagna, Irene Giardina, Francesco Ginelli *Phys. Rev E.* **89**, 042707 (2014)

- [45] Iva Pritišanac, Robert M. Vernon, Alan M. Moses , **21**, 662 (2019)
- [46] C. E. SHANNON The Bell System Technical Journal, **27**, pp. 379–423, 623–656 (1948)
- [47] Information, Entropy, Life and the Universe Arieh Ben-Naim (The Hebrew University of Jerusalem, Israel)10.1142/9479 — May 2015
- [48] J. Hebner and D. Osborn, Kumbha Mela: The World's Largest Act of Faith (Mandala Publishing Group, New York, 1991).
- [49] M. Specia, Hajj Begins as Muslims Flock to Mecca, The New York Times Aug. 09 (2019).
- [50] Jay Prakash Singh et al 2021 J. Phys. A: Math. Theor. in press